Covalent organic frameworks for extremely high reversible CO_2 uptake capacity: a theoretical approach†

Yoon Jeong Choi, Jung Hoon Choi, Kyung Min Choi and Jeung Ku Kang*

Received 31st August 2010, Accepted 21st October 2010
DOI: 10.1039/c0jm02891f

We report that the novel covalent organic frameworks (COFs) are capable of reversibly providing an extremely high uptake capacity of carbon dioxide at room temperature. These COFs are designed *via* the combination of *ab initio* calculations and force-field calculations. For this goal, we explore the adsorption sites of carbon dioxide on COFs, their porosity, as well as carbon dioxide adsorption isotherms. We identify the binding sites and energies of CO_2 on COFs using *ab initio* calculations and obtain the carbon dioxide adsorption isotherms using grand canonical ensemble Monte Carlo calculations. Moreover, the calculated adsorption isotherms are compared with the experimental values in order to build the reference model in describing the interactions between the CO_2 and the COFs and in predicting the CO_2 adsorption isotherms of COFs. Finally, we design three new COFs, 2D COF-05, 3D COF-05 (*ctn*), and 3D COF-05 (*bor*), for the high capacity CO_2 storage. The carbon dioxide adsorption values of the new 3D COFs are about six times larger than that of MOF-177. This suggests that 3D COFs are very promising candidates for high capacity CO_2 storage.

Introduction

Carbon dioxide is one of the greenhouse gases, which could result in global environmental problems such as climate change and the ocean acidification. Meanwhile, carbon dioxide can be utilized as a source of carbon for the future sustainable production of fuels, such as methane, methanol, and formaldehyde using for example artificial photosynthesis, thus, the development of technologies for carbon dioxide storage materials is essential for the carbon dioxide emission reduction and utilization.[1,2] Among these technologies, porous nanostructures are being considered as emerging materials.[3–5] In this view, the covalent organic frameworks (COFs) having both highly microporous and also mesoporous structures are of great interest due to their suitable porosity as well as their thermal stability and low density.[6–17] Furukawa and Yaghi have reported an experimental study on the gases' (H_2, CO_2, and methane) adsorption capacity of COFs, and very recently, Lan *et al.* have shown theoretically that the doping of metals in porous COFs provides an efficient approach for enhancing CO_2 capture.[11,18] However, despite these advantages of COFs, there is still a great obstacle in designing and searching for the novel COF nanostructure allowing a very high CO_2 uptake capacity at the practically usable room temperature. A deep understanding of the CO_2 adsorption in COFs is obviously a prerequisite for the design of new COFs with high CO_2 storage.

NanoCentury KAIST Institute, Graduate School of EEWS (WCU), Department of Materials Science and Engineering, Korea Advanced Institute of Science & Technology, 373-1, Guseong Dong, Yuseong Gu, Daejeon, 305-701, Republic of Korea. E-mail: jeungku@kaist.ac.kr; Fax: +82-42-350-1701; Tel: +82-42-350-1700

† Electronic supplementary information (ESI) available: Pore diameter of COF-10, atomic charges, snapshot of CO_2 located between two COF layers, binding sites and energies (in kcal mol^{-1}) of COF-8, COF-10, and TP-COF, the density distribution of CO_2 in COF-5, COF-8, COF-10, and TP-COF, crystal lattice parameters of COFs. See DOI: 10.1039/c0jm02891f

Here, we focus on designing novel COFs capable of reversibly providing the extremely high uptake capacity of carbon dioxide at room temperature. To achieve this goal, we perform a systematic theoretical study of carbon dioxide adsorptions on COFs using a combination of the *ab initio* calculations and force-field based calculations. We first identify the organic linkers with the adsorption sites suitable to capture carbon dioxide on COFs. Two-dimensional (2D) COFs, COF-5, COF-8, COF-10, and TP-COF, which were already synthesized, are selected as the target compounds.[6,8,19] The adsorption sites of carbon dioxide on these COFs and their porosity as well as carbon dioxide adsorption isotherms are determined. Then, the simulated results are compared with the experimental observations in order to provide the simulation reference model in an accurate determination of CO_2 adsorption properties on COFs. Finally, we extend 2D COFs to three-dimensional (3D) COFs and design new COFs providing high uptake capacities of carbon dioxide at room temperature.

Computational details

Adsorption sites of carbon dioxide on COFs

We have modelled four molecules for four 2D COFs (COF-5, COF-8, COF-10, and TP-COF) composed of one organic linker unit and one corner linker unit of each crystalline COF at the density functional level of theory (DFT) using Becke's three parameter hybrid functional with the Lee–Yang–Parr correlation functional (B3LYP).[20,21] The atomic charges have been also evaluated by applying the natural population analysis (NPA) to the fully optimized geometries.[22,23] The geometries of four molecules and CO_2 adsorbed on molecules have been determined through full geometry optimizations with no symmetry constraints using B3LYP calculations. Single-point second-order Møller–Plesset perturbation theory (MP2) energy calculations have also been carried out on the DFT optimized geometries. We

used the 6-31 + G* basis set for all atoms of models and the 6-311 + G* basis set for C and O atoms of carbon dioxide molecule. All DFT and MP2 calculations have been carried out using the Gaussian 03 program package.[24]

Crystalline and porous structures of COFs

Crystalline structures of COFs have been minimized using the DREIDING force-field, which has proven to be very accurate in reproducing structures of MOFs and COFs.[12,15,16,25] All force-field calculations have been performed using the forcite module of the Materials Studio 4.1 software suite.[26] On optimized crystalline porous COF structures, we have determined the two kinds of the surface areas, the Connolly surface area and the accessible surface area, pore volumes, pore diameters, and free volumes. A probe diameter of N_2 (0.3681 nm) was applied to determine the surface area and the total free volume. The accessible surface area and the total free volume of each COF have been calculated using the "Atoms Volume and Surface" calculation with 0.75 Å grid interval implemented in the Materials Studio 4.1 package.[26] Pore volumes in $cm^3\ g^{-1}$ were determined by dividing the total free volume by the cell volume and the cell density. Pore diameters were estimated by considering the smallest distances between two opposing hydrogen atoms of the phenyl groups in organic linker units. Fig. S1 in the ESI† illustrates the case of a COF-10.

Carbon dioxide adsorption isotherms

Carbon dioxide sorption isotherms for COFs have also been evaluated using the grand canonical ensemble Monte Carlo (GCMC) method implemented in MUSIC code *via* atomistic models of the adsorbents and the carbon dioxide molecules.[27] The adsorbent model is an infinite three-dimensional periodic super cell, $2 \times 2 \times 6$ for COFs of each unit cell. These supercells of COFs have six layers. The carbon dioxide molecules have been modelled using the elementary physical model (EPM) which had been successfully applied for the MOF–CO_2 interactions.[28] In the EPM model, the CO_2 molecule has a linear and fixed bond length C–O of 1.161 Å and the point charges of +0.6645*e* and −0.33225*e* on the carbon and oxygen atoms, respectively.[28a] The dispersion and repulsion interactions within all atoms have been modelled using the standard Lennard-Jones (LJ) equation.

$$V(r) = 4\varepsilon\left[\left(\frac{\sigma}{r}\right)^{12} - \left(\frac{\sigma}{r}\right)^{6}\right] \quad (1)$$

The LJ parameters in eqn (1) have been taken from the DREIDING force-field for the framework atoms and experiments for CO_2 molecules.[25,28] Lorentz–Berthelot mixing rules have been employed to calculate adsorbate/framework parameters. LJ interactions beyond 10.16, 10.38, 10.33, and 10.36 Å for COF-5, COF-8, COF-10, and TP-COF structures, respectively, have been neglected, which are the half values of each lattice parameter *a*.

For each point on the isotherm, 7 000 000 Monte Carlo steps have been performed for carbon dioxide, respectively, in GCMC simulations. Each step consisted of the insertion of a new molecule, deletion of an existing molecule, or translation of an existing molecule. Typically, the first half of the run is used for equilibration and the last half is used to calculate the ensemble averages.

The excess amount of the carbon dioxide, which can be reversibly stored and released, is obtained using eqn (2):

$$N_{ex} = N_{abs} - \rho_{(T,P)}V_{free} \quad (2)$$

where N_{abs} is the absolute adsorbed amount; that is, the total number of adsorbate carbon dioxide molecules present in the pore, N_{ex} is the excess adsorbed amount, $\rho_{(T,P)}$ is the density of carbon dioxide at the given temperature and pressure, and V_{free} is the free volume for the COFs.[29,30]

Results and discussion

Our work can be divided into five main parts: (1) identifying organic linkers with adsorption sites of carbon dioxide on COFs *via* the *ab initio* DFT and the MP2 methods, (2) characterizing the crystalline porous structures of 2D COFs, (3) obtaining CO_2 adsorption isotherms for 2D COFs, (4) extending to the 3D COFs, and (5) designing novel 3D COFs.

Adsorption sites of CO_2 on COFs

COFs are created as a result of the condensation reactions of 2,3,6,7,10,11-hexahydroxytriphenylene (HHTP) with 1,4-benzenediboronic acid (BDBA), 1,3,5-benzenetris(4-phenylboronic acid) (BTPA), 4,4′-biphenyldiboronic acid (BPDA), and pyrene-2,7-diboronic acid (PDBA) for COF-5, COF-8, COF-10 and TP-COF, respectively.[6,8,19] According to the molecular building block approach, HHTP molecules act as corner units, while BDBA, BTPA, BPDA, and PDBA molecules act as linker units. For *ab initio* calculations, we modelled each COF as a molecule composed of one corner unit and one linker unit. The fully optimized geometries at the DFT level for COF-5, COF-8, COF-10, and TP-COF model structures are given in Fig. 1. These molecules form planar structures by the hydrogen bonding between the B–O and H of phenyl rings except for COF-10, which is on a slightly twisted structure due to the twisted biphenyl group of BPDA. In general, although carbon dioxide has no dipole moment, it still has a quadrupole moment due to the charge separation in C═O bonds, thereby resulting in quadrupole–dipole interactions and quadrupole-induced dipole interactions between carbon dioxide and sorbent molecules. In these interactions, carbon dioxide can act simultaneously as both

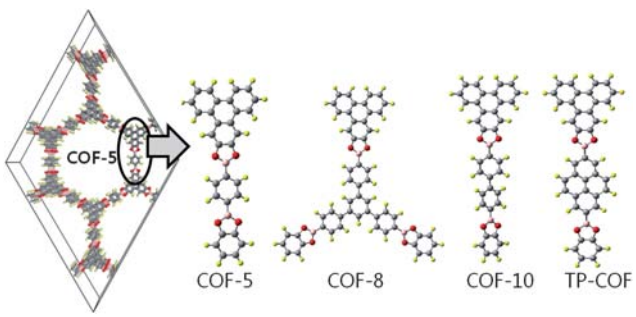

Fig. 1 Four model molecules for COF-5, COF-8, COF-10, and TP-COF.

Lewis acid (electron acceptor: C-interactive site) and also Lewis base (electron donor: O-interactive site).

To identify the binding sites of carbon dioxide, we first analyzed the atomic charges of molecules using the natural bonding orbital method, as described in Fig. S2, ESI†.[22,23] Boron and hydrogen atoms of COFs having positive atomic charges can interact with the O atoms of CO_2, while phenyl rings and oxygen atoms of COFs having negative atomic charges can interact with the C atom of CO_2. Based on this analysis, we generated the initial binding structures between CO_2 and COF-5 for further DFT optimization. The optimized binding structures and MP2 binding energies of CO_2 and COF-5 are presented in Fig. 2. The binding energy (E_b) between the adsorbed CO_2 and the COFs is defined as:

$$E_b = E\{nCO_2/COFs\} - E\{(n-1)CO_2/COFs\} - E\{CO_2\} \quad (3)$$

where n denotes the number of the adsorbed CO_2 molecules, while $E\{CO_2/COFs\}$ and $E\{CO_2\}$ denote the energies of the CO_2–COF complexes, and the CO_2 molecule, respectively. Energies were obtained using single-point MP2 energy calculations on DFT optimized structures. The eight predicted carbon dioxide binding sites and binding energies to the O (Fig. 2a), B (Fig. 2b), phenyl rings (Fig. 2c), and H (Fig. 2d), respectively, are described. The most preferable binding sites are located at the oxygen atom, as shown in Fig. 2a. In this case, CO_2 firstly interacts with the oxygen of B–O in COF-5, and secondly with adjacent boron or hydrogen atoms of the phenyl ring in COF-5. The binding energy of the O atom of CO_2 to the B atom of COF-5 is -1.7 kcal mol^{-1} (Fig. 2b, left), whereas the binding energy of CO_2 to the B and O atoms of COF-5 is -4.4 kcal mol^{-1} (Fig. 2b, right) with -2.7 kcal mol^{-1} from the additional binding energy due to neighboring O atoms in COF-5. A phenyl ring of the BDBA linker unit in COF-5 can bind carbon dioxide with -3.8 kcal mol^{-1} of binding energy (Fig. 2c, left), while the phenyl rings of HHTP corner unit do not exert a specific effect on the carbon dioxide affinity (-0.3 kcal mol^{-1}, Fig. 2c, right), thus implying that the modification of the linker unit can improve the CO_2 binding capacity of COFs. In a 2D layered crystalline structure, the CO_2 bound is located between two layers with -9.2 kcal mol^{-1} of binding energy, as displayed in Fig. S3, ESI†. After the first CO_2 molecule binds to the oxygen atom of B–O in COF-5, as described above in Fig. 2a, another carbon dioxide molecule can bind to the oxygen atom of the adsorbed CO_2 on COFs, which is displayed in Fig. 2e and f. The second CO_2 binding energies are determined to be -2.2 to -4.2 kcal mol^{-1}, values considerably larger than the value of -0.2 kcal mol^{-1} between two single CO_2 molecules. Accordingly, it is interpreted that once one CO_2 molecule binds to the COF-5, the adsorbed carbon dioxide can be used as the next binding. A similar binding trend was also observed for COF-8, COF-10, and TP-COF, as illustrated in Fig. S4, ESI†.

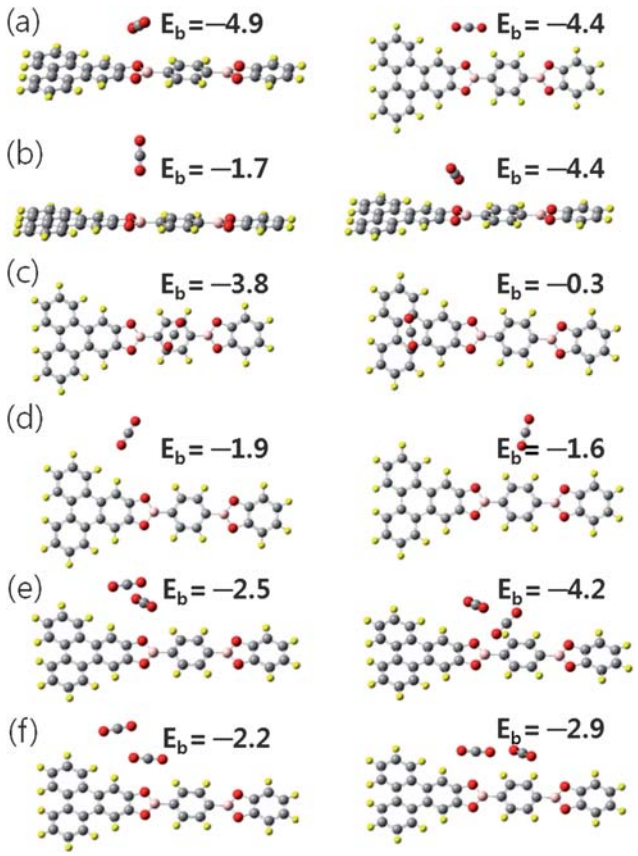

Fig. 2 Calculated binding sites and MP2 energies (E_b in kcal mol^{-1}) of CO_2 to (a) oxygen, (b) boron, (c) phenyl ring, (d) hydrogen, and (e and f) CO_2 adsorbed in a COF-5 model molecule (C in gray, O in red, B in pink, and H in yellow).

Crystalline and porous structures of 2D COFs

Using the force-field method, we calculated the crystalline structures of 2D COFs. Fully optimized crystalline structures and experimental values are summarized in Table S1†. COF-8 has the *P6/m*2 space group, while the space group symmetry of the others is *P6/mmm*. The geometry difference of 0.08 Å between the experimental and the calculated lattice parameters for TP-COF is very small, although the difference of 0.56 Å for COF-8 is a little larger. On these optimized crystalline geometries, we determined the surface areas (SAs), the pore volume, the pore diameter, and the percent free volume for each structure (Table 1). Two different methods of Connolly SA and accessible SA were used to calculate the SAs.[33,34] These physical properties can be used to determine the small molecule storage characteristics.[35] We found that our calculated accessible SAs are closer to experimental values. The experimental SAs for the COF-5 and the MOF-5 are 1670 (and 1590) and 3362 m^2 g^{-1}, which agree well with the predicted values of 1721 and 3383 m^2 g^{-1}, respectively.[6,11,31] For COF-8 and COF-10, calculated SAs are 1528 and 1908 m^2 g^{-1}, while the measured SA_{BET} values are 1350 and 1760 m^2 g^{-1}, respectively.[8] However, the measured SA of 868 m^2 g^{-1} for the TP-COF was somehow different from our calculated SA of 1760 m^2 g^{-1}.[19] Since a TP-COF with a larger pyrene linker would have a larger SA than a COF-5 with a benzene linker, the difference between the experimental and theoretical SA values could be attributed to the purification process used to obtain and prepare the pure experimental sample.[35] The percent free volume is defined as the percent ratio of the free volume to the total volume; COF-10 shows the best value among the 2D COFs of more than 70% in a percent free

Table 1 Porous structure data of COFs

Material	Connolly SA/m^2 g^{-1}	Accessible SA/m^2 g^{-1}	Pore volume/cm^3 g^{-1}	Free volume (%)	Pore diameter/nm
COF-5	1979	1721 (1670[a],1990[a])	1.16	65.1	2.6
COF-10	2116	1908 (1760[a], 2080[a])	1.59	72.4	3.3
TP-COF	1948	1760 (868[b])	1.34	66.5	3.1
COF-8	1970	1528 (1350[a], 1400[a])	0.79	56.1	1.8
MOF-5	3127	3383 (3362[c], 4400[d])	1.21	76.9	1.2
COF-102	4497	5203(3620[a], 4650[a])	1.82	75.7	1.2
COF-108	4420	6553	5.27	90.8	
2D COF-05	2338	2071	1.90	75.6	3.7
3D COF-05 (*bor*)	5003	8416	14.44	96.3	
3D COF-05 (*ctn*)	4987	8469	12.68	95.8	2.9

[a] Experimental value from ref. 11. [b] Experimental value from ref. 19. [c] Experimental value from ref. 31. [d] Experimental value from ref. 32.

volume. The minimum pore diameter sizes of 2D COFs range from 1.8 nm (for the COF-8) to 3.3 nm (for the COF-10). COF-10 exhibits the best porosity characteristics.

COF-5, COF-8, COF-10, and TP-COF have a 2D layered sheet structure with an interlayer distance of around 3.4 Å. This implies that carbon dioxide cannot be stored in this small interlayer space. For 2D COFs, the phenyl rings of both the HHTP molecule and the linker unit could be binding sites for the CO_2. Fig. S5a in the ESI† describes the density distribution (red dots) of CO_2 adsorbed in COF-5 at a fixed loading of 50, 100, 200, and 300 CO_2 molecules per $2 \times 2 \times 6$ cell. At a low CO_2 coverage, the main CO_2 adsorption sites are located near the oxygen atoms and the additional CO_2 adsorption could occur above CO_2 adsorbed on COFs with a high CO_2 coverage, consistent with those of the results from *ab initio* calculations. Consequently, the pore size, the volume, and the surface area, in addition to oxygen atoms in COFs, could be also major factors that influence the CO_2 uptake capacities of COFs. We also illustrated the cases of COF-8, COF-10, and TP-COF in Fig. S5b, ESI†.

Adsorption isotherms of CO_2 in 2D COFs

Carbon dioxide sorption isotherms for COFs at 298 K were also determined using the GCMC method as presented in Fig. 3. The calculated and experimental data of COFs at 55 bar and 298 K are summarized in Table 2.[11] The MOF-5 is used as a reference.

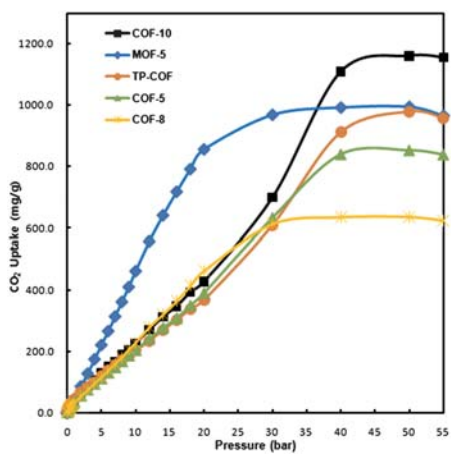

Fig. 3 Carbon dioxide adsorption isotherms of 2D COFs at 298 K.

Table 2 The carbon dioxide uptakes at 55 bar and 298 K of COFs

COFs	CO_2 uptakes/mg g^{-1}	Error percent (%)
COF-10	1155 (1010[a])	14
TP-COF	959	
COF-5	838 (870[a])	−4
COF-8	625 (630[a])	−1
MOF	966 (968[b])	−0.2
COF-102	1230 (1200[a])	2.5
COF-108	3784	
2D COF-05	1360	
3D COF-05 (*bor*)	9285	
3D COF-05 (*ctn*)	8582	

[a] Experimental value from ref. 11. [b] Experimental value from ref. 36.

For comparison, we define the error percentage as the difference between the calculated and the experimentally measured values divided by the measured value. The error percentages are found to be −4, −1, and 14% for COF-5, COF-8, and COF-10, respectively. The CO_2 uptake capacities of COF-8 and COF-10 are found to be 625 and 1155 mg g^{-1}, consistent with experimental and other simulated results.[11,16] Also, the calculated excess CO_2 uptake capacity on MOF-5 of 966 mg g^{-1} is proven to agree with the experimental value of 968 mg g^{-1}.[36] This demonstrates that interaction potentials used in this work and force-field approach are reliable and useful in predicting CO_2 adsorption isotherms in COFs. COF-10 shows the capacity of above 1000 mg g^{-1}, while COF-8 with the smallest surface area produces the smallest saturated CO_2 uptake capacity value. At low and medium pressures, the slope of the carbon dioxide uptake capacities for COF-8 having the smallest pore size is raised steeply and is saturated at 30–40 bar, but the CO_2 uptake capacities for COFs having large pore diameter are saturated slowly with higher values at higher pressures. This relationship between the pore diameter and saturation pressure of COFs is similar to those of MOFs.[11,31,37] Our calculated carbon dioxide isotherms of 2D COFs achieve saturation near 45 bar. The CO_2 uptake capacities for COFs are listed in decreasing order: COF-10 > TP-COF > COF-5 > COF-8.

Extending to 3D COFs

According to our *ab initio* and GCMC results, the oxygen atoms in COFs are the primary binding sites while the phenyl rings of

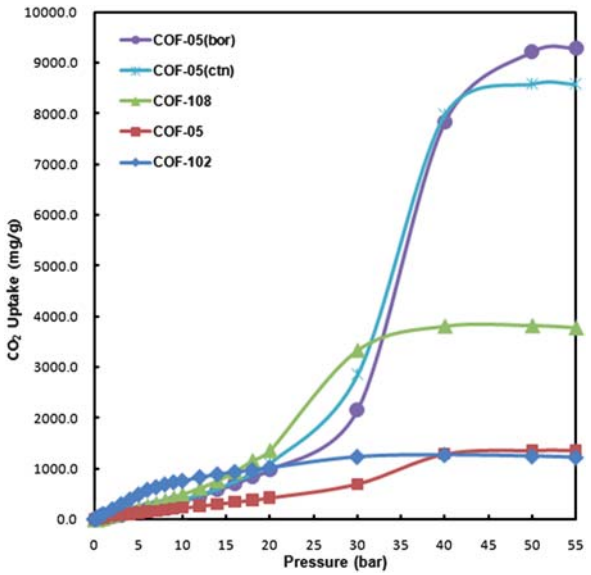

Fig. 4 Carbon dioxide adsorption isotherms of 3D COFs at 298 K.

linker units and the CO_2 bound in COFs are the second strong binding sites. For the effective CO_2 adsorptions in COFs, the edges and faces of pores should be fully accessible, however, the phenyl rings of linker units in 2D COFs are not fully utilized due to the layered structures of 2D COFs. In this view, we also studied two representative 3D COFs, COF-102 and COF-108, which are created by a self-condensation reaction of the tetrahedral tetra(4-dihydroxyborylphenyl)methane (TBPM) with $I\bar{4}3d$ (*ctn*) symmetry and by a condensation reaction of TBPM and HHTP with cubic space group symmetry $P\bar{4}3m$ (*bor*).[8] We determined the porosity structures and carbon dioxide adsorption isotherms of these two 3D COFs using the force-field method. Surface areas, pore sizes, pore volumes, percent free volumes and carbon dioxide uptake values at 55 bar and 298 K for COF-102 and COF-108 are presented in Tables 1 and 2 and Fig. 4. The experimental CO_2 saturation uptake value of 1200 mg g^{-1} for our reference structure of COF-102 is observed by the 1230 mg g^{-1} calculated in this work. For COF-108, the carbon dioxide uptake value is 3784 mg g^{-1} at 55 bar, larger than those for MOF-5 (970 mg g^{-1}) and MOF-177 (1490 mg g^{-1}). Also, it is three times larger than that for COF-102. Compared with 2D COF-5 having the same building units (HHTP and BDBA), 3D COF-108 shows about 3.8 times larger surface areas, about a 4.5 times larger pore volume, about a 26% larger percent free volume, and about 4.5 times larger CO_2 saturation uptakes. At the low and medium pressures, COF-102 exhibits a higher CO_2 storage capacity than COF-108, but, as the pressure increases above 20 bar, COF-108 has a high CO_2 uptake capacity of up to 3784 mg g^{-1} at 55 bar. It means that larger SAs and pore volumes of COFs yield higher CO_2 saturation values, thereby showing that COFs having large pore volume and SAs can be promising candidates for the high capacity CO_2 storage.

Newly designed COFs

Based on the above results and a molecular building block approach, we designed the new 3D COFs for novel CO_2 storages

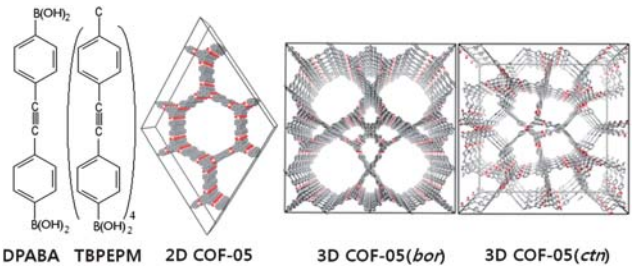

Fig. 5 Structures for DPABA, TBPEPM, 2D COF-05, 3D COF-05 (*bor*), and 3D COF-05 (*ctn*).

by modifying linker units. We selected a diphenylacetylene-4,4′-diboronic acid (DPABA) molecule for 2D COFs and a tetrahedral tetra[4-(4-dihydroxyborylphenyl)ethynyl]phenyl methane (TBPEPM) for 3D COFs, respectively, as a linker unit because two benzene rings of DPABA and TBPEPM form large pores and the central acetylene group makes it planar. We designed new 2D COF-05 using HHTP (corner unit) and DPABA (linker unit) and 3D COF-05(*ctn*) and COF-05(*bor*) using HHTP (corner unit) and TBPEPM (linker unit) (Fig. 5 and Table S2†). We also calculated the porous structures and CO_2 uptake properties of these new COFs, and the results are summarized in Tables 1 and 2 and Fig. 4. 2D COF-05 has slightly larger (~10%) SAs and pore diameter and a 20% larger pore volume compared with COF-10; when compared with COF-102, it has about half of the SAs, a three times larger pore diameter, a 10% larger pore volume, but a similar percent free volume. In terms of the CO_2 uptake capacities, 2D COF-05 can store a higher CO_2 than COF-10 by about 20% and 10% higher than COF-102. The shape of CO_2 adsorption isotherm for 2D COF-05 is the same as that of COF-10, but the CO_2 saturation uptake value of 2D COF-05 is increased in proportion as the pore volume is increased. Two 3D COF-05 structures exhibit around 30% wider SAs and 5% higher percent free volumes than the case of COF-108. These also have 2.4 to 2.7 times larger and 7 to 8 times larger pore volumes than those for COF-108 and COF-102, respectively. For CO_2 saturation uptake values at 55 bar, 3D COF-05 (*ctn*) and COF-05 (*bor*) also have 2.3 to 2.5 times higher and 7 to 7.5 times higher than those for COF-108 and COF-102, respectively.

Conclusions

We investigated the crystalline, porous structures and carbon dioxide adsorption isotherms of the 2D and 3D COFs using *ab initio* (DFT and MP2) and GCMC methods. We found that carbon dioxide acting both as Lewis acid and also Lewis base can bind to oxygen atoms and phenyl rings of linker units in COFs. Neighboring boron and hydrogen atoms of phenyl rings in COFs enhance the binding of CO_2 to COFs. The calculated carbon dioxide adsorption isotherms *via* the GCMC method agree well with the observed values from experimental values for 2D and 3D COFs, thus showing that our force-field method is suitable for describing the interactions between the CO_2 and the COFs and is useful for predicting the CO_2 adsorption isotherms of COFs. This work provides a reference model for the study of CO_2 adsorption in COFs. The most preferable binding site is located at the oxygen atom in COFs and the adsorbed CO_2 in

COFs can be the next binding site. We found that the CO_2 saturation uptake of 2D COFs is proportional to the surface areas and pore volumes. In 3D COFs, the phenyl rings of linker units are fully accessible, and this facilitates the effective CO_2 binding to COFs. We also found that COF-108 has the highest CO_2 capacity among the reported COFs, with a value of 3784 mg g^{-1}. In addition, we designed three new 2D COF-05, 3D COF-05 (*ctn*), and 3D COF-05 (*bor*) for high capacity CO_2 storages. In particular, the CO_2 saturation uptake value at 298 K and 55 bar is 8582 mg g^{-1} for 3D COF-05 (*ctn*) and 9285 mg g^{-1} for 3D COF-05 (*bor*). These carbon dioxide adsorption values are about six times larger than those of MOF-177 and COF-102. Consequently, it is concluded that 3D COFs are promising candidates for the high capacity CO_2 storage, and this work will stimulate other researchers to develop novel carbon dioxide storage materials with high uptake capacities.

Acknowledgements

This work was primarily supported by the Korea Center for Artificial Photosynthesis (KCAP), funded by the Ministry of Education, Science and Technology (NRF-2009-C1AAA001-2009-0093879), by the Hydrogen Energy R&D Center from one of the 21st Century Frontier R&D Programs, and by the WCU program (R-31-2008-000-10055-0). Dr Y. J. Choi's fellowship was supported by the Priority Research Centers Program (NRF-2009-0094041) and Basic Science Research Program (NRF-2009-0069987). Also, Mr J. H. Choi, and Mr K. M. Choi were supported in part by grants from the National Research Foundation (NRF-R0A-2007-000-20029-0) and the Center for Inorganic Photovoltaic materials (NRF-2010-0007692).

References

1 M. Mikkelsen, M. Jørgensen and F. C. Krebs, *Energy Environ. Sci.*, 2010, **3**, 43.
2 D. M. D'Alessandro, B. Smit and J. R. Long, *Angew. Chem., Int. Ed.*, 2010, **49**, 6058.
3 H. K. Chae, D. Y. Siberio-Pérez, J. Kim, Y.-B. Go, M. Eddaoudi, A. J. Matzger, M. O'Keeffe and O. M. Yaghi, *Nature*, 2004, **427**, 523.
4 Y. Liu, J. F. Eubank, A. J. Cairns, V. C. Kravtsov, R. Luebke and M. Eddaoudi, *Angew. Chem., Int. Ed.*, 2007, **46**, 3278.
5 S. Ma and H. C. Zhou, *Chem. Commun.*, 2010, **46**, 44.
6 A. P. Côté, A. Benin, N. Ockwig, M. O'Keeffe, A. Matzger and O. M. Yaghi, *Science*, 2005, **310**, 1166.
7 H. M. El-Kaderi, J. R. Hunt, J. L. Mendoza-Cortés, A. P. Côté, R. E. Taylor, M. O'Keeffe and O. M. Yaghi, *Science*, 2007, **316**, 268.
8 A. P. Côté, H. M. El-Kaderi, H. Furukawa, J. R. Hunt and O. M. Yaghi, *J. Am. Chem. Soc.*, 2007, **129**, 12914.
9 J. R. Hunt, C. J. Doonan, J. D. LeVangie, A. P. Côté and O. M. Yaghi, *J. Am. Chem. Soc.*, 2008, **130**, 11872.
10 F. J. Uribe-Romo, J. R. Hunt, H. Furukawa, C. Klőck, M. O'Keeffe and O. M. Yaghi, *J. Am. Chem. Soc.*, 2009, **131**, 4570.
11 H. Furukawa and O. M. Yaghi, *J. Am. Chem. Soc.*, 2009, **131**, 8875.
12 G. Garberoglio, *Langmuir*, 2007, **23**, 12154.
13 Y. J. Choi, J. W. Lee, J. H. Choi and J. K. Kang, *Appl. Phys. Lett.*, 2008, **92**, 173102.
14 S. S. Han, H. Furukawa, O. M. Yaghi and W. A. Goddard, III, *J. Am. Chem. Soc.*, 2008, **130**, 11580.
15 G. Garberoglio and R. Vallauri, *Microporous Mesoporous Mater.*, 2008, **116**, 540.
16 R. Babarao and J. W. Jiang, *Energy Environ. Sci.*, 2008, **1**, 139.
17 E. Klontzas, E. Tylianakis and G. E. Froudakis, *Nano Lett.*, 2010, **10**, 452.
18 J. Lan, D. Cao, W. Wang and B. Smit, *ACS Nano*, 2010, **4**, 4225.
19 S. Wan, J. Guo, J. Kim, H. Ihee and D. Jiang, *Angew. Chem., Int. Ed.*, 2008, **47**, 8826.
20 A. D. Becke, *J. Chem. Phys.*, 1993, **98**, 5648.
21 C. T. Lee, W. T. Yang and R. G. Parr, *Phys. Rev. B: Condens. Matter Mater. Phys.*, 1988, **37**, 785.
22 A. E. Reed and F. Weinhold, *J. Chem. Phys.*, 1983, **78**, 4066.
23 A. E. Reed, R. B. Weinstock and F. Weinhold, *J. Chem. Phys.*, 1985, **83**, 735.
24 M. J. Frisch, G. W. Trucks, H. B. Schlegel, G. E. Scuseria, M. A. Robb, J. R. Cheeseman, J. A. Montgomery, Jr, T. Vreven, K. N. Kudin, J. C. Burant, J. M. Millam, S. S. Iyengar, J. Tomasi, V. Barone, B. Mennucci, M. Cossi, G. Scalmani, N. Rega, G. A. Petersson, H. Nakatsuji, M. Hada, M. Ehara, K. Toyota, R. Fukuda, J. Hasegawa, M. Ishida, T. Nakajima, Y. Honda, O. Kitao, H. Nakai, M. Klene, X. Li, J. E. Knox, H. P. Hratchian, J. B. Cross, V. Bakken, C. Adamo, J. Jaramillo, R. Gomperts, R. E. Stratmann, O. Yazyev, A. J. Austin, R. Cammi, C. Pomelli, J. W. Ochterski, P. Y. Ayala, K. Morokuma, G. A. Voth, P. Salvador, J. J. Dannenberg, V. G. Zakrzewski, S. Dapprich, A. D. Daniels, M. C. Strain, O. Farkas, D. K. Malick, A. D. Rabuck, K. Raghavachari, J. B. Foresman, J. V. Ortiz, Q. Cui, A. G. Baboul, S. Clifford, J. Cioslowski, B. B. Stefanov, G. Liu, A. Liashenko, P. Piskorz, I. Komaromi, R. L. Martin, D. J. Fox, T. Keith, M. A. Al-Laham, C. Y. Peng, A. Nanayakkara, M. Challacombe, P. M. W. Gill, B. Johnson, W. Chen, M. W. Wong, C. Gonzalez and J. A. Pople, *Gaussian 03, Revision C.02*, Gaussian, Inc., Wallingford CT, 2004.
25 S. Mayo, B. Olafson and W. A. Goddard, III, *J. Phys. Chem.*, 1990, **94**, 8897.
26 *Material Studio 4.1*, Accelrys Software Inc, 2006.
27 A. Gupta, S. Chempath, M. J. Sanborn, L. A. Clark and R. Q. Snurr, *Mol. Simul.*, 2003, **29**, 29.
28 (*a*) G. H. Jonathan and H. Y. Kwong, *J. Phys. Chem.*, 1990, **94**, 8897; (*b*) S. Babarao and J. Jiang, *Langmuir*, 2008, **24**, 6270.
29 A. V. Neimark and P. I. Ravikovitch, *Langmuir*, 1997, **13**, 5148.
30 Thermophysical Properties of Fluid Systems, in *NIST Chemistry Webbook*, http://webbook.nist.gov/chemistry/fluid/, 2008.
31 J. L. C. Rowsell, A. R. Millward, K. S. Park and O. M. Yaghi, *J. Am. Chem. Soc.*, 2004, **126**, 5666.
32 S. S. Kaye, A. Dailly, O. M. Yaghi and J. R. Long, *J. Am. Chem. Soc.*, 2007, **129**, 14176.
33 M. L. Connolly, *J. Appl. Crystallogr.*, 1983, **16**, 548.
34 T. Düren, F. Millange, G. Férey, K. S. Walton and R. Q. Snurr, *J. Phys. Chem. C*, 2007, **111**, 15350.
35 H. Frost, T. Düren and R. Q. Snurr, *J. Phys. Chem. B*, 2006, **110**, 9565.
36 A. R. Millward and O. M. Yaghi, *J. Am. Chem. Soc.*, 2005, **127**, 17998.
37 K. S. Walton, A. R. Millward, D. Dubbeldam, H. Frost, J. J. Low, O. M. Yaghi and R. Q. Snurr, *J. Am. Chem. Soc.*, 2008, **130**, 406.

